Supporting Information

Superior high-rate capability of $Na_3(VO_{0.5})_2(PO_4)_2F_2$ nanoparticles embedded in porous graphene through pseudocapacitive effect

Xingde Xiang, Qiongqiong Lu, Mo Han, and Jun Chen*

S1. Experimental section

S1.1. Materials synthesis

Graphene oxide (GO) solution (8.3 mg ml^{-1}) was firstly prepared through oxidizing graphite powder with a modified Hummers method.[1, 2]

The $Na_3(VO_{0.5})_2(PO_4)_2F_2$/graphene was synthesized by using a sample solid-state route, with an initial molar ratio (3: 2: 2: 3) of Na, V, P, and F elements in starting materials. Typically, 0.5 g vanadium pentoxide (V_2O_5, 99%) and 1.04 g oxalate dehydrate ($H_2C_2O_4 \cdot 2H_2O$, 99.5%) were added into 40 ml distilled water. The suspension was covered with a plastic-film and then magnetically stirred at 80 °C until transparent VOC_2O_4 was formed. 0.633 g ammonium dihydrogen phosphate ($NH_4H_2PO_4$, 99%) and GO solution with required amount were added. After 10 minutes, the solution was evaporated and further dried at 80 °C overnight to produce the mixture of VOC_2O_4, $NH_4H_2PO_4$ and reduced graphene oxide. After sufficiently ground by hand, the powder mixture was transferred into a furnace with Ar-fluxing and treated at 350 °C for 4 h and at 650 °C for 6 h to form vavadium phosphates precursor. Desired $Na_3(VO_{0.5})_2(PO_4)_2F_2$/graphene was finally obtained by reacting the precursor with sodium fluoride (NaF, 0.37 g, 98%) in Ar atmosphere at 600 °C for 2 h. In order to investigate the effect of GO dosage on particle size, specific area and pore volume of the $Na_3(VO_{0.5})_2(PO_4)_2F_2$/graphene, various GO dosages (0 ml, 5 ml, 10 ml, 15 ml) were utilized, and corresponding products were respectively denoted as NVPF-0ml (pristine

$Na_3(VO_{0.5})_2(PO_4)_2F_2$ in manuscript), NVPF-5ml, NVPF-10ml, and NVPF-15ml ($Na_3(VO_{0.5})_2(PO_4)_2F_2$/graphene in manuscript).

S1.2. Materials characterization

The structures of the materials were analyzed with X-ray diffraction (Rigaku MiniFlex600, Cu *K*α radiation). The morphology was observed by using field-emission scanning electron microscopy (SEM, JEOL JSM7500F), transmission electron microscopy (TEM, JEOL 2100F), and N_2 adsorption/desorption measurement (BELSORP-mini instrument, 77 K). The actual composition was estimated by using ICP analysis and EDX measurements. The EDX measurement was undertaken at a selected area.

S1.3. Electrochemical measurements

The cathode electrode was fabricated by coating an uniform slurry of 70 wt% active material ($Na_3(VO_{0.5})_2(PO_4)_2F_2$/graphene), 20 wt% conductive agent (Super P carbon) and 10 wt% binder (polyvinylidene fluoride, PVDF) onto an Al foil. The electrode loading of the active materials is 1.1~1.2 mg cm^{-2}. 2032-type cells was assembled by using Na metal as the anode, glass fiber as the separator and 1 M $NaClO_4$/EC-PC (1: 1, *v*/*v*, 5 wt% FEC) as the electrolyte. The electrochemical performance was measured with galvanostatic charge and discharge on Land test system. The cyclic voltammetry was performed on the same electrode one after the other at various scanning rates. The electrochemical impedance spectra were measured at 3.7 V in the frequency range of 100 kHz and 10 mHz, with an amplitude of 10 mV.

S2. Synthesis optimization

In this work, our target is to synthesize nanosized NVPF particles embedded in porous graphene as superior cathode material for sodium-ion batteries. The nanosizing of the NVPF crystals can shorten the diffusion pathway and increase the diffusion interface of Na^+ ions, while the porous graphene can enhance the electrolyte infiltration and electron conductivity of

the material. However, too much graphene would sacrifice the specific capacity of the NVPF/graphene material owing to the electrochemical inactivity of the graphene at high potentials (>2.0 V *vs* Na^+/Na). Hence, we design the particle size as the primary parameter for optimizing the material synthesis.

S2.1. Effect of GO dosage on particle size

Figure S1 shows XRD patterns of NVPF-0ml, NVPF-5ml, NVPF-10ml, and NVPF-15ml samples. As observed, the peak positions are not changed with altering the GO dosage, suggesting that the GO dosage has no influence on crystal structure of the materials. It should be mentioned that the peaks are continuously broadened with increasing the GO dosage possibly due to reduction of particle size. In order to confirm the reduction, their particle sizes have been estimated by using Scherrer equation: $d = k\lambda / \beta \cos\theta$, where d is the particle size (nm), k is Scherrer constant (0.89), λ is the wavelength (0.154056 nm) of X-ray, β is the peak width (rad) at half height, and θ is the scattering angle. Here, the (222) peak is chosen for the calculation owing to no overlap with other peaks, and the calculated results are listed in **Table S**1. Obviously, the GO addition reduces the size of the NVPF particles. However, the particle size can't be further reduced when the dosage increases to 15 ml. Hence, the 15 ml is considered to be the optimum GO dosage, equivalent to 0.25 g GO per 1 g V_2O_5 precursor.

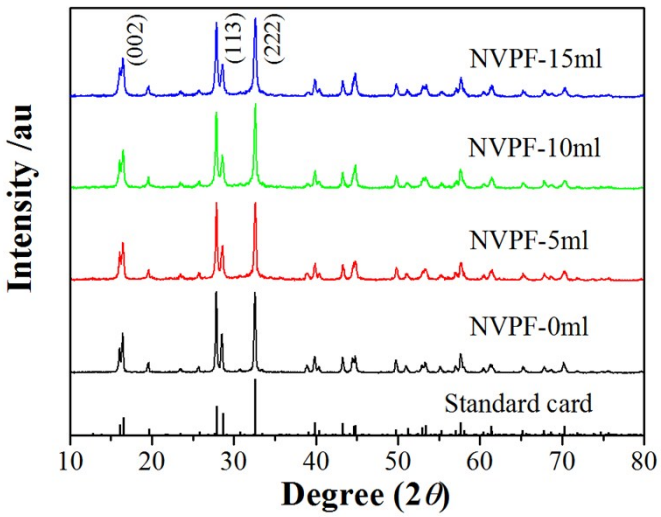

Figure S1. XRD patterns of NVPF-0ml, NVPF-5ml, NVPF-10ml and NVPF-15ml.

Table S1 Calculated particle size of those NVPF samples based on Scherrer equation.

Sample	2θ for (222) peak	HWHM	Particle size
NVPF-0ml	32.6°	~0.182°	~45 nm
NVPF-5ml	32.6°	~0.232°	~35 nm
NVPF-10ml	32.6°	~0.256°	~32 nm
NVPF-15ml	32.6°	~0.274°	~30 nm

S2.2. Effect of GO dosage on material morphology

Figure S2 shows the SEM images of NVPF-0ml, NVPF-5ml, NVPF-10ml, and NVPF-15ml samples. As observed, the NVPF prepared without GO addition is composed of large aggregates. With increasing GO dosage, the particles are being dispersed, and the graphene network is being increased.

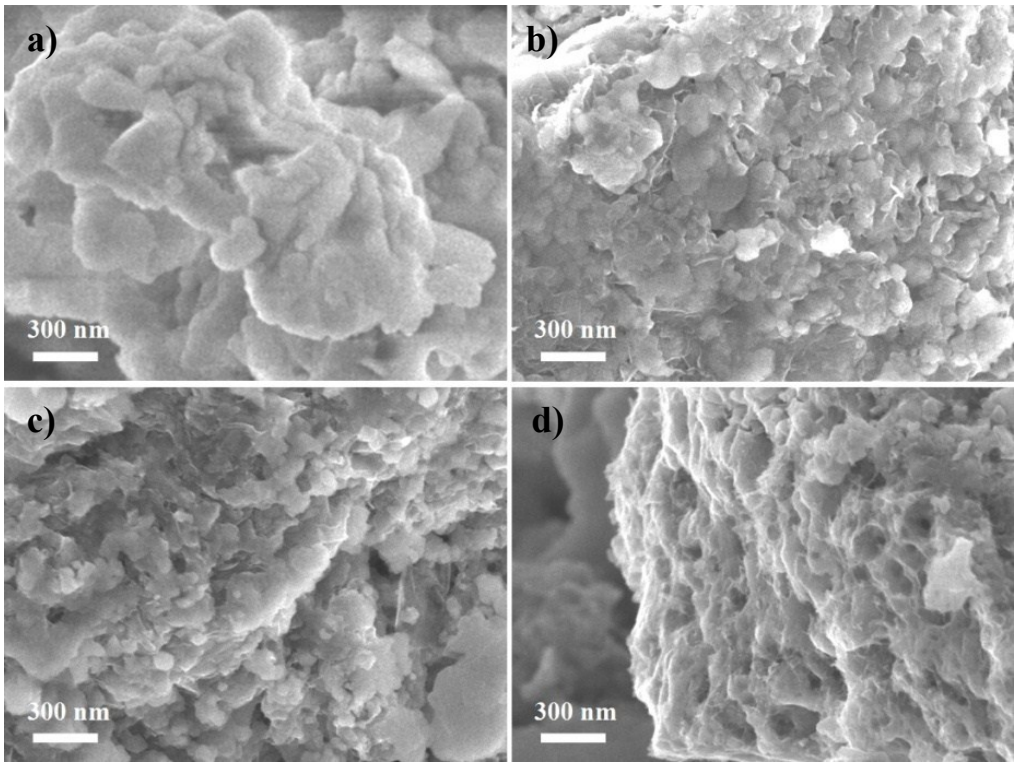

Figure S2. SEM images of a) NVPF-0ml, b) NVPF-5ml, c) NVPF-10ml, and d) NVPF-15ml.

S2.3. Effect of GO dosage on specific area and pore volume

Figure S3 shows the N2-adsorption/desorption curves of NVPF-0ml, NVPF-5ml, NVPF-10ml, and NVPF-15ml samples. As seen, the NVPF prepared without GO addition has a small specific area and a negligible pore volume. With increasing the GO dosage, the specific area and pore volume significantly increase due to reduction of NVPF particle size and increase of graphene network. Although NVPF-10ml and NVPF-15ml samples have similar particle sizes, the specific area and pore volume of NVPF-15ml sample are much larger than those of NVPF-10ml sample owing to increase of graphene content. In addition, the pore diameter is not changed with altering the GO dosage, suggesting that the pore in the materials mainly originates from the graphene network.

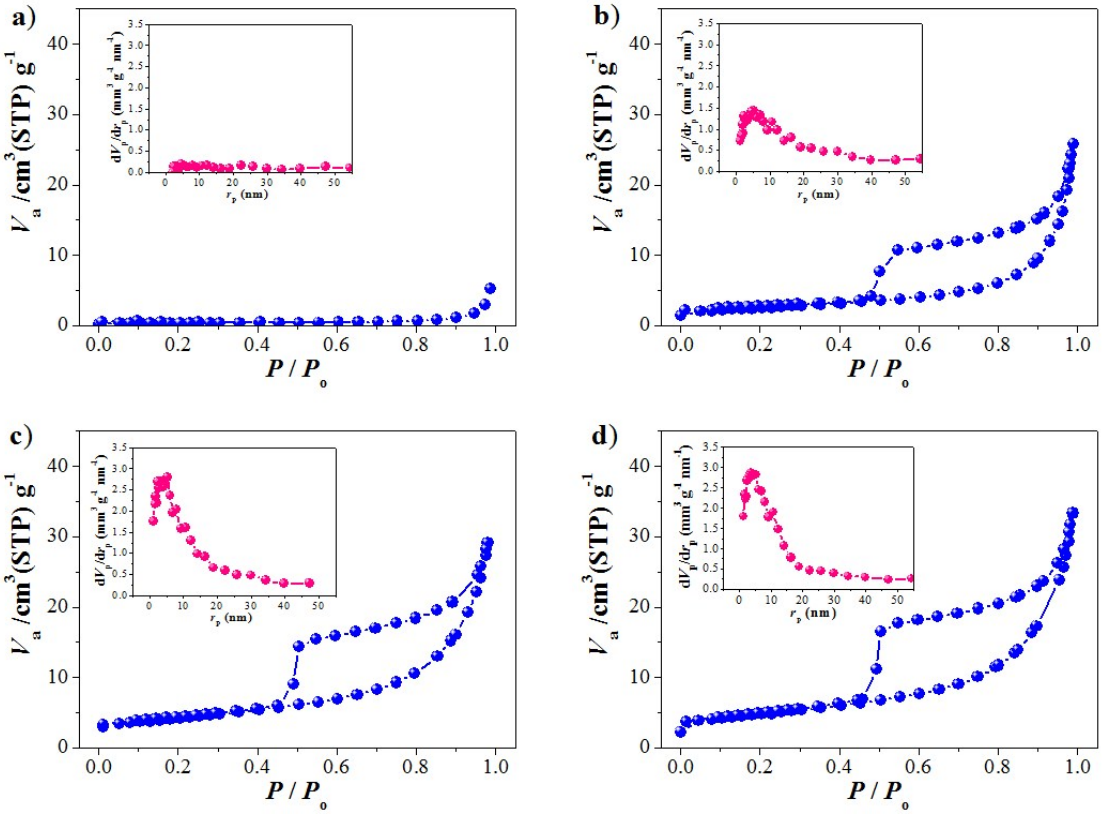

Figure S3. N_2-adsorption/desorption curves and pore distributions (inset) of a) NVPF-0ml, b) NVPF-5ml, c) NVPF-10ml, and d) NVPF-15ml.

Table S2. Specific areas and pore volumes of those samples

Sample	BET area /m^2 g^{-1}	Pore volume / m^3 g^{-1}
NVPF-0ml	~1.34	~0.31
NVPF-5ml	~8.57	~1.97
NVPF-10ml	~14.6	~3.34
NVPF-15ml	~16.5	~3.78

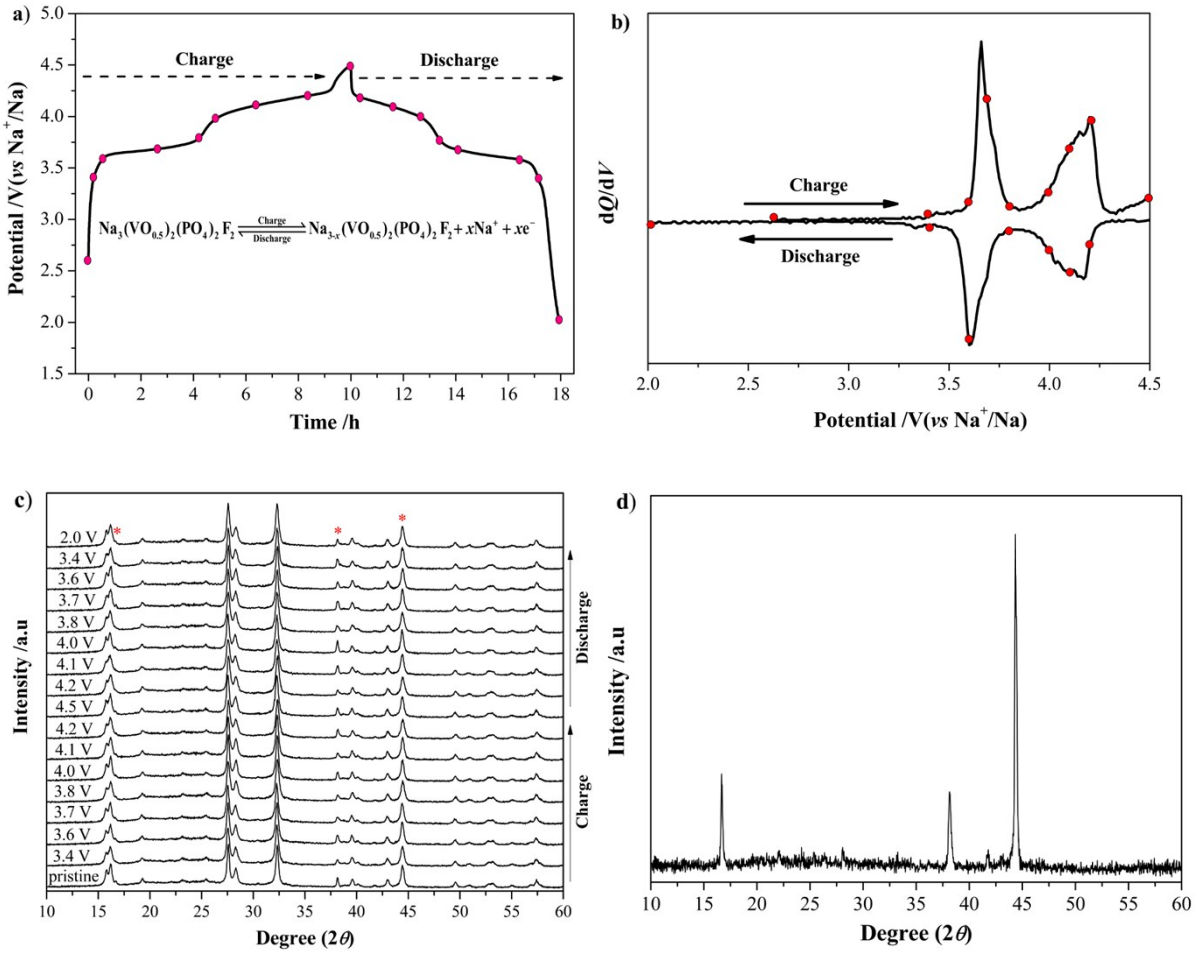

Figure S4. Reaction mechanism of the $Na_3(VO_{0.5})_2(PO_4)_2F_2$/graphene: a) charge/discharge curves, b) dQ/dV curves, c) ex-situ XRD profiles at various states of charge/discharge (the

asterisk represents the background peaks belonging to Al foil/adhesive), and d) XRD profile of Al foil/adhesive.

S3. Charge/discharge properties

S3.1. Reaction mechanism

In order to investigate the reaction mechanism of the $Na_3(VO_{0.5})_2(PO_4)_2F_2$/graphene during charge/discharge process, we have tested its charge/discharge curves at a relatively low current rate of 0.1 C and identified the main reaction regions. As seen from the dQ/dV curve shown in **Figure S**4b, there are one couple of weak peaks (~3.4 V) and two couples of strong peaks (~3.65 V and ~4.1 V) for oxidation/reduction of vanadium. **Figure S**4c shows the ex-situ XRD of the material at various states of charge/discharge (corresponding to the 17 points in Figure S4a and Figure S4b). As observed, with altering the state of charge/discharge, the $Na_3(VO_{0.5})_2(PO_4)_2F_2$/graphene material does not exhibit disappearance of original peaks and appearance of new peaks. This suggests that the NVPF/graphene material undergoes a single-phase reaction during Na deintercalation/intercalation, consistent with previous reports on the $Na_3(VO)_2(PO_4)_2F$ and $Na_3V_2(PO_4)_2F_3$ materials.[3, 4] The appearance of three plateaus during the single-phase reaction can be attributed to the rearrangement of Na ions at Na1 site and Na2 site with deintercalation/intercalation of Na ions, which does not change the overall crystal structure. As proposed by Dunn' group,[5] the structure that doesn't undergo phase transformation during ion intercalation is an important design rule for intercalation pseudocapacitance.

S3.2. Cycling performance

Figure S5a shows the differential curves (dQ/dV) of the $Na_3(VO_{0.5})_2(PO_4)_2F_2$/graphene. As seen, those redox peaks don't show observable change with extended cycling, implying highly reversible Na deintercalation/intercalation process. As exhibited in **Figure S5**b, the

$Na_3(VO_{0.5})_2(PO_4)_2F_2$/graphene material shows a reversible capacity of 100 mAh g^{-1} at the first cycle and retains a capacity of 91 mAh g^{-1} after 200 cycles. The capacity retention is 91%, much higher than that of the pristine $Na_3(VO_{0.5})_2(PO_4)_2F_2$. With an aim to understand the improved cycling performance, we have investigated the crystal structure of the cycled materials. As compared in **Figure S**6, the pristine $Na_3(VO_{0.5})_2(PO_4)_2F_2$ exhibits obvious shift of XRD peaks, while the $Na_3(VO_{0.5})_2(PO_4)_2F_2$/graphene material doesn't show any observable shift. The result suggests that the $Na_3(VO_{0.5})_2(PO_4)_2F_2$/graphene material has an enhanced structural stability possibly due to the carbon coating that protects the active $Na_3(VO_{0.5})_2(PO_4)_2F_2$ from side reaction with electrolytes. In addition, as seen from **Figure S**7, the cycled $Na_3(VO_{0.5})_2(PO_4)_2F_2$/graphene material still keeps the particle size of about 30 nm and the (002) spacing of ~0.53 nm, further confirming the good structural and morphological stabilities.

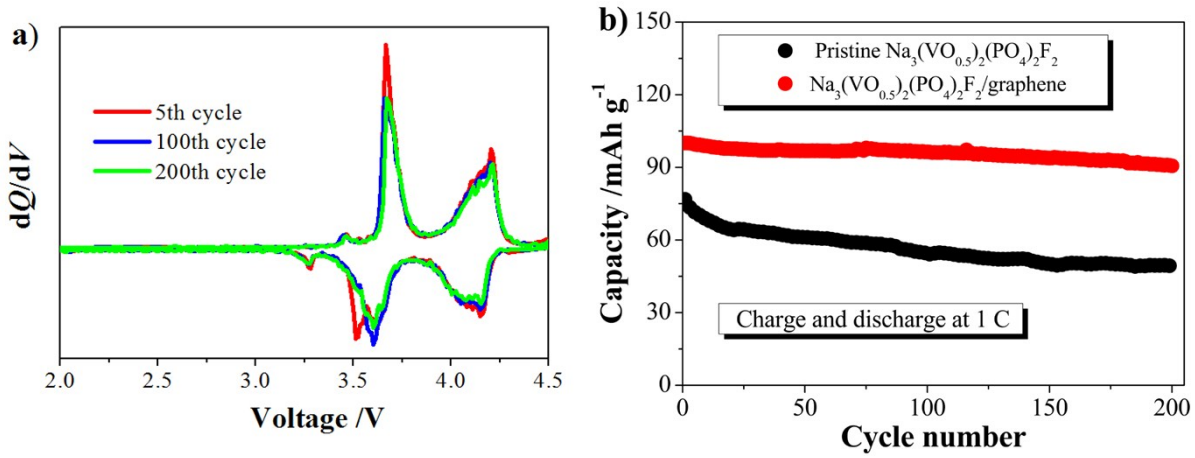

Figure S5. a) dQ/dV profiles of the $Na_3(VO_{0.5})_2(PO_4)_2F_2$/graphene, and b) variations of discharge capacity *vs* cycle number of the $Na_3(VO_{0.5})_2(PO_4)_2F_2$/graphene and $Na_3(VO_{0.5})_2(PO_4)_2F_2$ at a charge/discharge rate of 1 C.

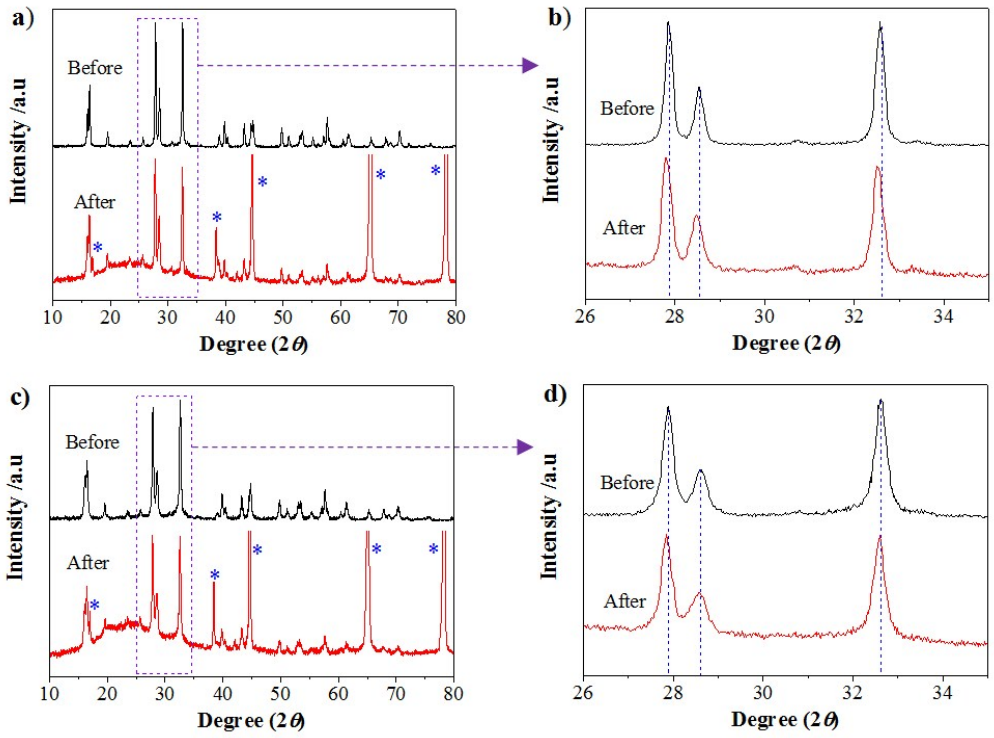

Figure S6. a-b) XRD patterns of the $Na_3(VO_{0.5})_2(PO_4)_2F_2$ before and after cycling 200 cycles, and c-d) XRD patterns of the $Na_3(VO_{0.5})_2(PO_4)_2F_2$/graphene before and after cycling 200 cycles. (The "*" symbol represents the backgroud peaks from Al foil and adhesive).

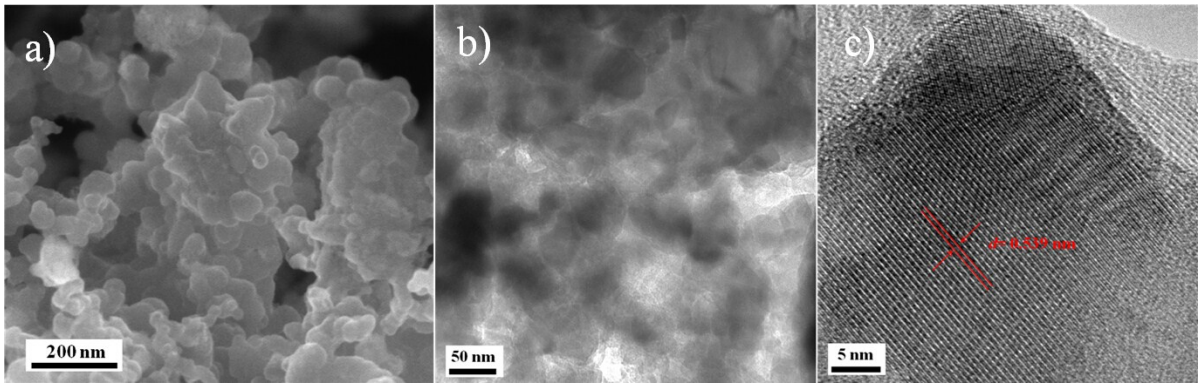

Figure S7. a) SEM image and b, c) TEM images of the cycled $Na_3(VO_{0.5})_2(PO_4)_2F_2$/graphene.

S3.3. Rate performance

S3.3.1. Discharge capacities at various C-rates

Figure S8 presents the discharge curves and Coulombic efficiency of the $Na_3(VO_{0.5})_2(PO_4)_2F_2$ and $Na_3(VO_{0.5})_2(PO_4)_2F_2$/graphene at various C-rates. As exhibited, the GO addition

significantly enhances the stability in the high-rate capability and coulombic effciency, due to facilitation of reaction kinetics.

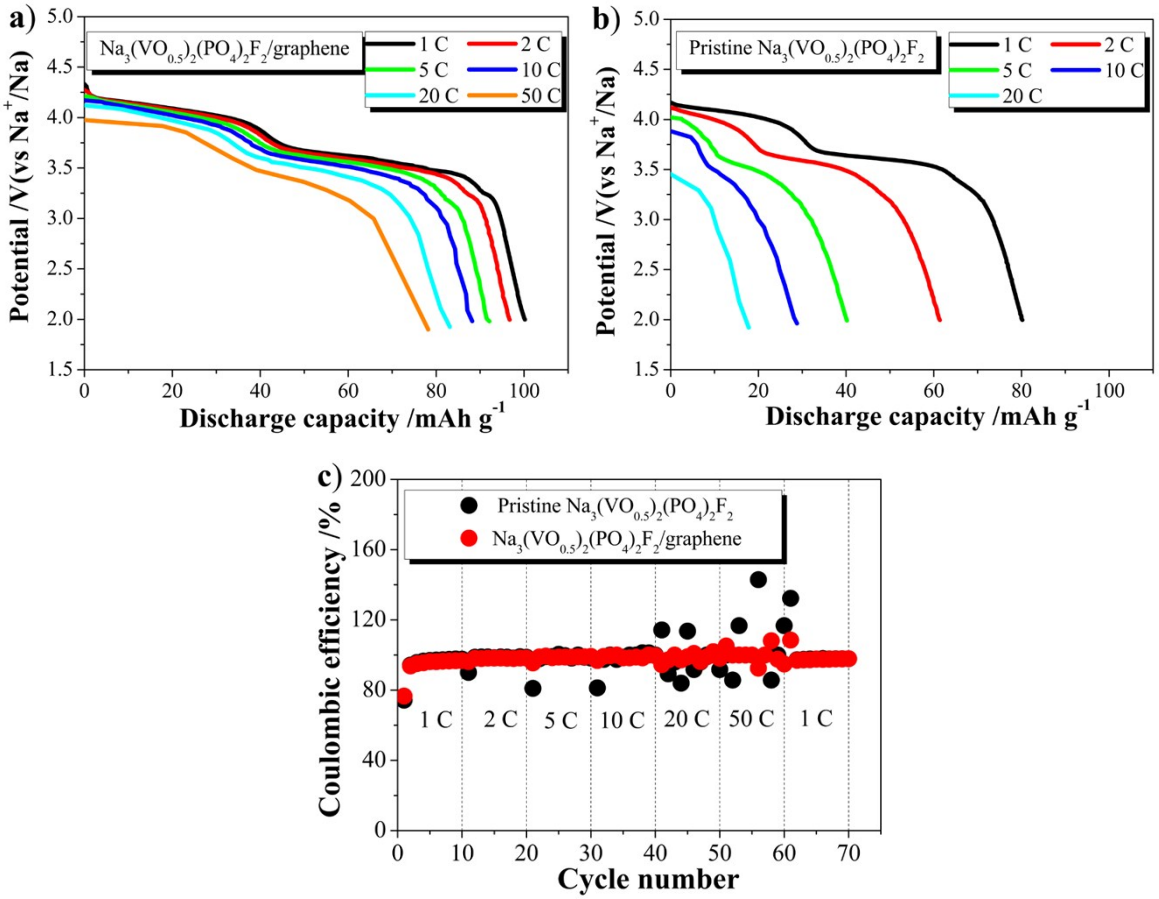

Figure S8. Discharge curves at various C-rates (a, b) and Coulombic efficiency (c) of the $Na_3(VO_{0.5})_2(PO_4)_2F_2$/graphene and $Na_3(VO_{0.5})_2(PO_4)_2F_2$.

S3.3.2. Reaction kinetics

Figure S9 shows the cyclic voltammograms of the $Na_3(VO_{0.5})_2(PO_4)_2F_2$ and $Na_3(VO_{0.5})_2(PO_4)_2F_2$/graphene at various scanning rates (0.1 mV s^{-1}, 0.2 mV s^{-1}, 0.3 mV s^{-1}, 0.5 mV s^{-1}, 0.7 mV s^{-1}, and 1.0 mV s^{-1}). According to the equation (1), it is found that the pristine $Na_3(VO_{0.5})_2(PO_4)_2F_2$ exhibits *b* values of close to 0.5, suggesting a diffusion-controlled reaction process, while the $Na_3(VO_{0.5})_2(PO_4)_2F_2$/graphene shows the *b* values of close to 1.0, indicating that the reaction process is dominated by capacitive effect.

Respective contributions of diffusion-controlled reaction and capacitive effect to the peak currents of the $Na_3(VO_{0.5})_2(PO_4)_2F_2$/graphene have been presented in Figure 4c, which are deconvoluted based on the equations (2-4).

$$i_p = av^b \quad (1)$$

$$i_c = SC_d v = k_1 v \quad (2)$$

$$i_r = 2.69 \times 10^5 Sn^{3/2} D_{Na}{}^{1/2} v^{1/2} C^0{}_{Na} = k_2 v^{1/2} \quad (3)$$

$$i_p = i_c + i_r = k_1 v + k_2 v^{1/2} \quad (4)$$

Where i_c and i_r respectively represent the currents contributed by capacitive effect and intercalation reaction, C_d is specific capacitance, D_{Na} is chemical diffusion coefficient of Na^+ ions in material bulk, S is surface area (103.95 cm^2), n is electron-transfer number, $C^0{}_{Na}$ is the bulk concentration (0.0075 mol cm^{-3}) of Na ions, k_1 and k_2 represent constant numbers.

Figure S10 shows the EIS spectra measured at various temperatures of the $Na_3(VO_{0.5})_2(PO_4)_2F_2$ and $Na_3(VO_{0.5})_2(PO_4)_2F_2$/graphene. The activation energy of charge-transfer reaction can be estimated based on the equations (5-6).

$$i_o = RT / nFR_{ct} \quad (5)$$

$$i_o = Ae^{-E_a/RT} \quad (6)$$

Where i_o is the exchange current, A is a temperature-dependent coefficient, R is gas constant, T is the absolute temperature, F is Faraday constant. According to the linear relationship of log (i_o) and $1/T$ (the inset), the apparent activation energy of $Na_3(VO_{0.5})_2(PO_4)_2F_2$/graphene is calculated to be ~39.5 kJ mol^{-1}, close to that of the pristine $Na_3(VO_{0.5})_2(PO_4)_2F_2$ (~44.2 kJ mol^{-1}). According to the knowledge of electrode reaction, it is known that the factors affecting the reaction kinetics consist of mass transfer, activation barrier and electron conductivity. Since the $Na_3(VO_{0.5})_2(PO_4)_2F_2$/graphene and $Na_3(VO_{0.5})_2(PO_4)_2F_2$ possess similar barrier values, the enhanced reaction kinetics of $Na_3(VO_{0.5})_2(PO_4)_2F_2$/graphene should be ascribed to

the improvement of mass transfer and electron conductivity. This is consistent with our analyses in the manuscript.

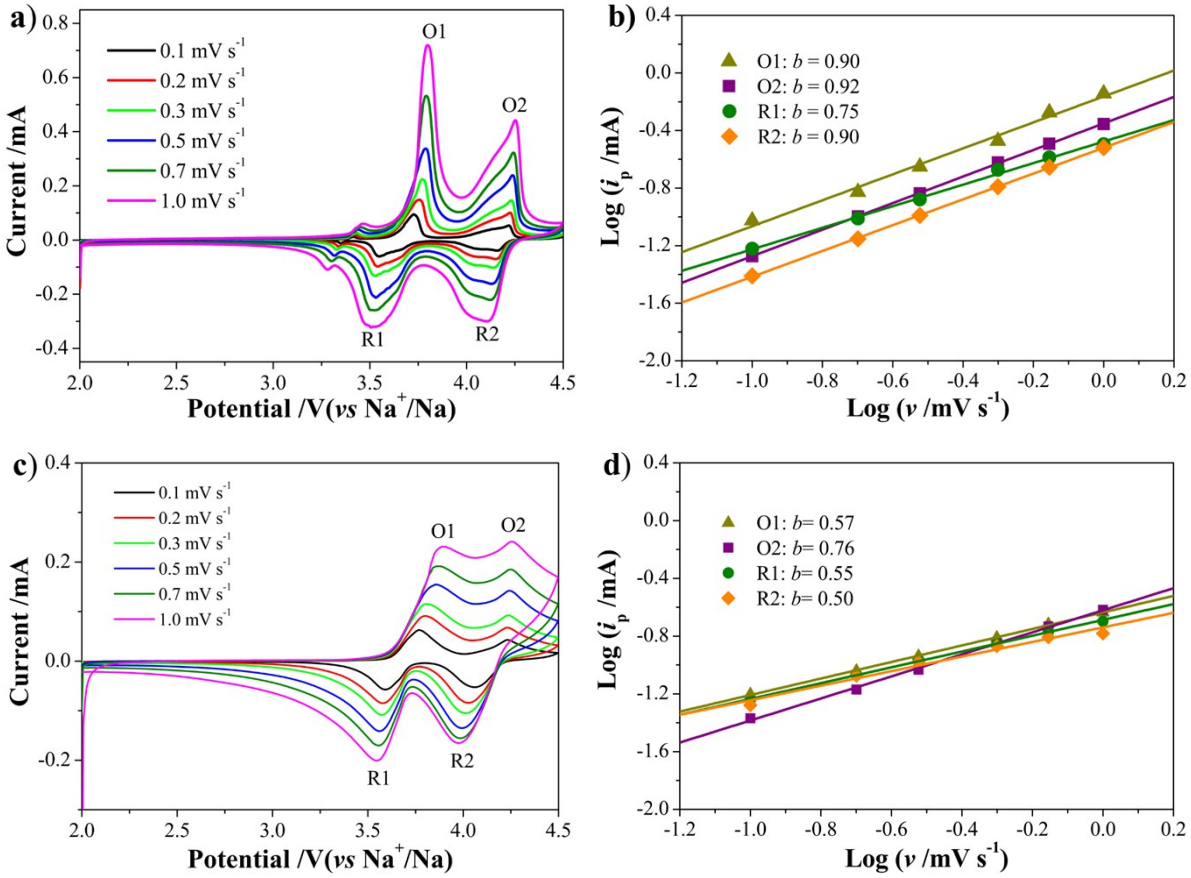

Figure S9. Cyclic voltammograms obtained at various scanning rates and linear relationships between log (i_p) and log (v) (inset) of the $Na_3(VO_{0.5})_2(PO_4)_2F_2$/graphene (a, b) and $Na_3(VO_{0.5})_2(PO_4)_2F_2$ (c, d).

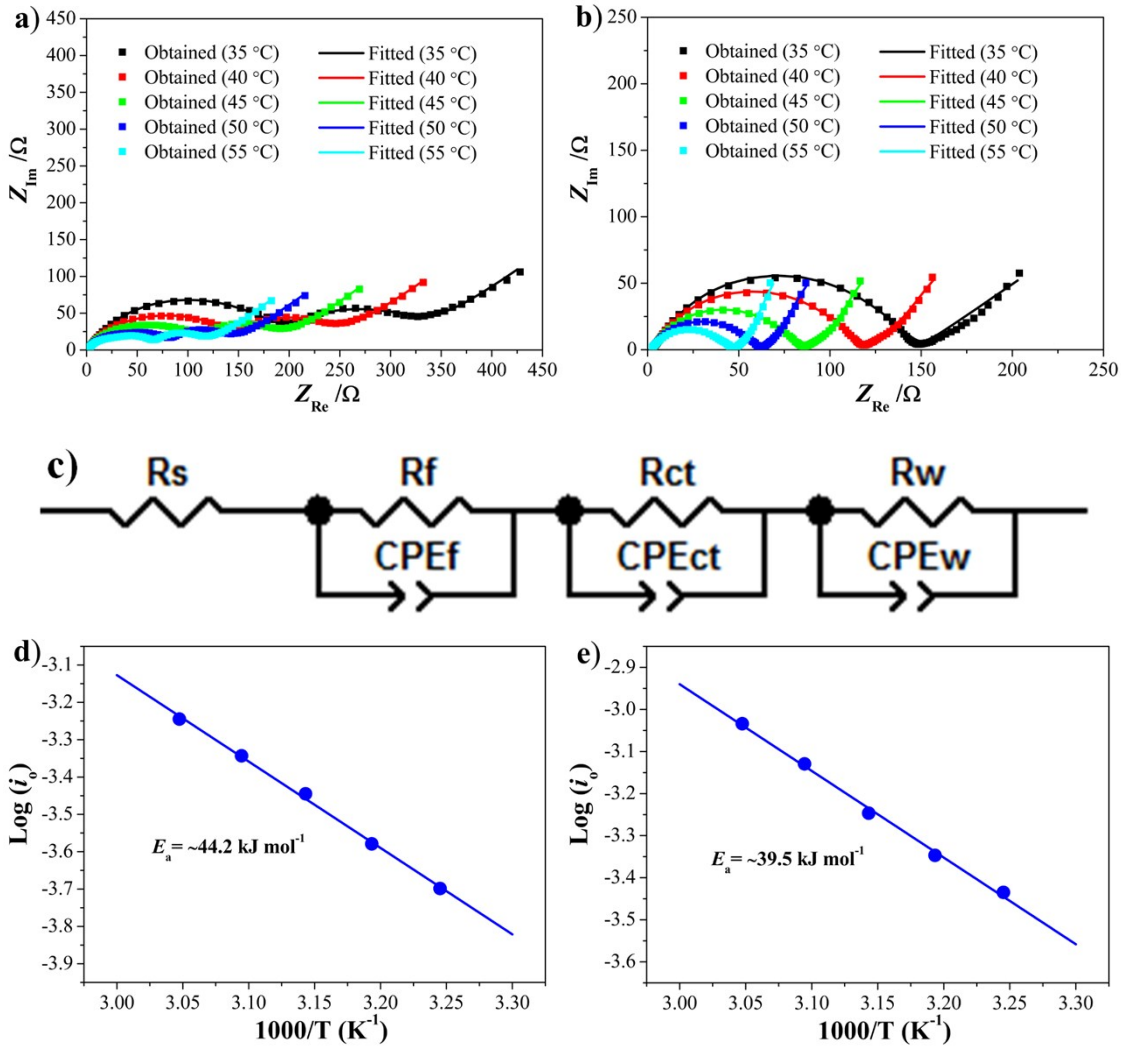

Figure S10. EIS spectra, equivalent circuit, and the relationship between log (i_o) and 1/T (inset) of the $Na_3(VO_{0.5})_2(PO_4)_2F_2$ (a, c, d) and $Na_3(VO_{0.5})_2(PO_4)_2F_2$/graphene (b, c, e).

Table S3. Obtained R_{ct} values for the $Na_3(VO_{0.5})_2(PO_4)_2F_2$ and $Na_3(VO_{0.5})_2(PO_4)_2F_2$/graphene.

Temperature /°C	**$Na_3(VO_{0.5})_2(PO_4)_2F_2$**	**$Na_3(VO_{0.5})_2(PO_4)_2F_2$/graphene**
~30	164.7	89.49
35	132.6	72.25
40	102.3	59.97
45	76.36	48.37
50	61.35	37.51
55	49.68	30.56

S3.3.3. Performance comparison with previous reports

Table S4. Performance comparison of the NVPF materials reported in literature and this work

Material	Particle size	Rate performance	Source
NVPF	~50 nm	73 mAh g^{-1} at 10 C	Ref. 6
NVPF/RuO_2	~50 nm (diameter)	71 mAh g^{-1} at 40 C	Ref. 3
NVPF/MWCNTs	~1.5μm	41 mAh g^{-1} at 20 C	Ref. 7
NVPF@C/graphene	~300 nm	78.5 mAh g^{-1} at 10 C	Ref. 8
NVPF/graphene	~300 nm	66 mAh g^{-1} at 5 C	Ref. 9
NVPF/C	~500 nm	68 mAh g^{-1} at 1 C	Ref. 10
NVPF/graphene	~30 nm	100 mAh g^{-1} at 1 C, 92 mAh g^{-1} at 5 C, 88 mAh g^{-1} at 10 C, 82 mAh g^{-1} at 20 C, 77 mAh g^{-1} at 50 C	This work

1. D. A. Dikin, S. Stankovich, E. J. Zimney, R. D. Piner, G. H. Dommett, G. Evmenenko, S. T. Nguyen and R. S. Ruoff, *Nature*, 2007, **448**, 457-460.
2. Z. Niu, L. Liu, L. Zhang, Q. Shao, W. Zhou, X. Chen and S. Xie, *Adv. Mater.*, 2014, **26**, 3681-3687.
3. M. H. Peng, B. A. Li, H. J. Yan, D. T. Zhang, X. Y. Wang, D. G. Xia and G. S. Guo, *Angew. Chem. Int. Ed.*, 2015, **54**, 6452-6456.
4. R. A. Shakoor, D. H. Seo, H. Kim, Y. U. Park, J. Kim, S. W. Kim, H. Gwon, S. Lee and K. Kang, *J. Mater. Chem.*, 2012, **22**, 20535-20541.
5. V. Augustyn, J. Come, M. A. Lowe, J. W. Kim, P. L. Taberna, S. H. Tolbert, H. D. Abruña, P. Simon and B. Dunn., *Nat. Mater.*, 2013, **12**, 518-522.

6. Y. Qi, L. Mu, J. Zhao, Y. S. Hu, H. Liu and S. Dai, *Angew. Chem. Int. Ed.*, 2015, **54**, 9911-9916.

7. P. R. Kumar, Y. H. Jung, C. H. Lim and D. K. Kim, *J. Mater. Chem. A*, 2015, **3**, 6271-6275.

8. H. Jin, J. Dong, E. Uchaker, Q. Zhang, X. Zhou, S. Hou, J. Li and G. Cao, *J. Mater. Chem. A*, 2015, **3**, 17563-17568.

9. M. W. Xu, L. Wang, X. Zhao, J. Song, H. Xie, Y. H. Lu and J. B. Goodenough, *Phys. Chem. Chem. Phys.*, 2013, **15**, 13032-13037.

10. P. Serras, V. Palomares, P. Kubiak, L. Lezama and T. Rojo, *Electrochem. Commun.*, 2013, **34**, 344-347.